We are IntechOpen, the world's leading publisher of Open Access books Built by scientists, for scientists

4,800
Open access books available

122,000
International authors and editors

135M
Downloads

Our authors are among the

154
Countries delivered to

TOP 1%
most cited scientists

12.2%
Contributors from top 500 universities

CLARIVATE ANALYTICS BOOK CITATION INDEX INDEXED

WEB OF SCIENCE™

Selection of our books indexed in the Book Citation Index in Web of Science™ Core Collection (BKCI)

Interested in publishing with us?
Contact book.department@intechopen.com

Numbers displayed above are based on latest data collected.
For more information visit www.intechopen.com

7

Low-Frequency Coherent Raman Spectroscopy Using Spectral-Focusing of Chirped Laser Pulses

Masahiko Tani[1], Masakazu Hibi[1], Kohji Yamamoto[1], Mariko Yamaguchi[2], Elmer S. Estacio[1], Christopher T. Que[1] and Masanori Hangyo[3]
[1]*Research Center for Development of Far-Infrared Region, University of Fukui,*
[2]*Graduate School of Materials Science, Nara Institute of Science and Technology,*
[3]*Institute of Laser Engineering, Osaka University*
Japan

1. Introduction

Vibrational spectroscopy is generally implemented using two schemes; that is, absorption spectroscopy and Raman spectroscopy. Conventionally, low frequency absorption spectroscopy is carried out using Fourier transform spectrometers equipped with a far infrared radiation source and a thermal detector. On the other hand, low frequency Raman spectroscopy is carried out by way of double or triple monochromaters and high-quality notch filters, whose performance determines the low frequency limit of the Raman spectrometer. In addition, in recent years, terahertz time-domain spectroscopy (THz-TDS) (Hangyo et al., 2005), utilizing femtosecond lasers as the excitation source, has been developed. THz-TDS enabled us to obtain absorption and dispersion spectra with a high signal-to-noise ratio in a frequency region less than 3 THz (100 cm^{-1}) and can be applied for absorption spectroscopy of various substances (Kawase et al., 2009; Korter et al., 2006; Taday et al., 2003;Tani et al., 2004; Tani et al., 2010; Walther et al., 2003; Yamamoto et al., 2005; Yamaguchi et al., 2005) and imaging measurements (Kawase, 2004).

There is a keen interest in low frequency vibrational spectroscopy for biomolecules since large amplitude, low frequency modes in macro biomolecules are believed to be associated with their respective function, as in the case of proteins (Chou, 1985, 1988). In order to fully understand the dynamics and function mechanisms of biomolecules, it is necessary to study their large amplitude and anharmonic low-frequency vibrational motions as these govern their thermal and physiochemical properties. A normal mode analysis of protein molecules revealed that large amplitude vibrational modes which are delocalized in the whole molecule lie within the THz region (< 120 cm^{-1}) (Brooks & Karplus, 1985; Go et al., 1983). In addition, the calculations suggested that the entropy of the whole molecule, specifically its thermodynamic characteristics, is governed by the large amplitude vibrational modes in the sub-THz region (<30 cm^{-1}). Consequently, important information related to the functions and dynamics of proteins can be derived by investigating THz vibration spectra.

For observation of low frequency vibrational modes in macro biomolecules, the absorption spectroscopy, including THz-TDS, has not been very successful because of the strong absorption of water in aqueous or hydrated samples. Low frequency Raman spectroscopy, on the other hand, seems to be promising for the study of low frequency vibrational modes in macro biomolecules since Raman spectroscopy is less influenced by water molecules as compared to THz absorption spectroscopy. As such, there have been some reports on the use of low frequency Raman spectroscopy to observe low frequency vibrational modes in proteins, such as lysozyme (Genzel et al., 1976; Urabe et al., 1998).

Some difficulties arise in carrying out the low frequency Raman or low frequency coherent Raman spectroscopy, in contrast to the high frequency regime; especially in the case of biological samples. One such problem is the strong Rayleigh scattering from rugged surfaces like powdered samples and from large biomolecules such as proteins and DNA. Therefore, to obtain a clear Raman spectrum, an efficient notch filter, such as the vapour iodine filter (Okajima & Hamaguchi, 2009), is required. In addition, slow signal fluctuations arising from thermal gradients due to laser beam heating also poses problems. To remove the thermal fluctuation, a noise subtraction technique using a lock-in amplifier has been reported (Genzel et al., 1976).

A more significant drawback in using Raman Spectroscopy, however, is its inherently low signal intensity. To overcome the low signal intensity in spontaneous Raman spectroscopy, coherent Raman techniques, such as Coherent Anti-Stokes Raman Scattering (CARS), may be utilized. Using the coherent Raman scattering, the signal can be increased by 5 to 6 orders of magnitude compared to that of spontaneous Raman scattering. With this high signal intensity, CARS from the C-H stretching mode has been successfully used for the molecular imaging of biological cells and tissues.

In line with this, the authors have recently developed coherent Raman spectroscopy technique in the THz frequency region aimed for imaging and spectroscopy of biomolecules. This technique uses a broadband femtosecond laser as the light source, as opposed to the customary nano- to picosecond monochromatic laser, in exciting the coherent Raman scattering and in detecting the signals in the time-domain. The femtosecond laser is advantageous since it can also be used in a THz-TDS system. At the moment, this technique is still being fully developed and has not been applied in the spectroscopy of biomolecules nor in the spectroscopic imaging of living tissues. The authors discuss the concept of the time-domain coherent Raman spectroscopy based on the "spectral focusing" technique. Furthermore, we demonstrate a series of proof-of-principle measurements by using a semiconductor sample. Observations on the optical phonon bands of GaSe in the THz frequency through the time-domain CARS and inverse Raman spectroscopy are presented. Lastly, efforts on the improvements in the signal-to-noise ratio (SNR) for future measurements of biomolecules are discussed.

2. Principle of the coherent Raman spectroscopy in terahertz frequency region using spectral focusing of femtosecond laser

2.1 Basics of coherent Raman spectroscopy

The basic principle of Raman scattering is explained briefly prior to discussing coherent Raman spectroscopy in the terahertz frequency region. A polarization $\boldsymbol{P}^{(1)}$ is induced when a molecule or crystal lattice is placed under an electric field, $\boldsymbol{E}_0$. The induced polarization depends linearly on the applied electric field through the polarizability α when the field is not so strong, and it can be described by

$$\boldsymbol{P}^{(1)} = \alpha \boldsymbol{E}_0. \quad (1)$$

In the above equation, the polarization $\boldsymbol{P}^{(1)}$ represents the polarization of one molecule, or the induced macroscopic polarization by the molecules or crystal lattice per unit volume. Additionally, the polarizability α is dependent on the molecule; hence any periodic change in the molecule from thermally excited molecular or lattice vibration, will also periodically change α. When a laser of frequency ω_0 with an electric field amplitude $\boldsymbol{E_0}$ is incident onto a material, wherein its constituent molecules fluctuate periodically at a vibration frequency $\delta\omega$, the polarization $\boldsymbol{P}^{(1)}$ will oscillate at the same frequency ω_0 of the incident laser and, at the same time, $\boldsymbol{P}^{(1)}$ will be modulated by the change in α induced by molecular vibrations. This will then lead to the sum frequency $\omega_0+\delta\omega$ and difference frequency $\omega_0-\delta\omega$. Specifically, the polarization $\boldsymbol{P}^{(1)}$ will oscillate with the three frequency components ω_0, $\omega_0+\delta\omega$, and ω_0 - $\delta\omega$. Since the emitted electromagnetic wave is proportional to the change in the electric polarization $\partial^2 P^{(1)} / \partial t^2$, light will be scattered by the molecule according to three mechanisms: (1) light with the same frequency as the incident light ω_0 (Rayleigh scattering), (2) positive shift $\omega_0+\delta\omega$ with the vibration frequency $\delta\omega$ (anti-Stokes), and (3) negative shift $\omega_0-\delta\omega$ with the vibration frequency $\delta\omega$ (Stokes). For thermally excited molecular vibrations, the vibration amplitude and phase is small and incoherent, respectively. Thus, the positive and negative interference of the emission from each molecule will occur with equal probabilities which prevents a large scattering intensity to be obtained. Also, the Stokes and anti-Stokes signals are relatively weak compared to the Rayleigh scattering. In this regard, an efficient notch filter and monochromator are needed in order to suppress the Rayleigh scattering. On top of this, a highly sensitive photomultiplier tube or CCD camera are needed to observe the weak Stokes and anti-Stokes signals. Additionally, it should be noted that the polarization $\boldsymbol{P}^{(1)}$ is a vector and since the polarization is dependent on the vector component of the incident electric field, the polarizability α is a tensor (Raman tensor). However, we will not consider its tensor properties at this time, for simplicity.

Now, let us consider a situation that two electric fields, $\boldsymbol{E_1}$ and $\boldsymbol{E_2}$ with frequencies ω_1 and ω_2, respectively are incident on the material in addition to $\boldsymbol{E_0}$. Three-wave mixing occurs with these two waves and $\boldsymbol{E_0}$, to induce a polarization $\boldsymbol{P}^{(3)}$. In this case we have

$$\boldsymbol{P}^{(1)} = \alpha \boldsymbol{E}_0\boldsymbol{E}_1\boldsymbol{E}_2 . \quad (2)$$

This nonlinear optical interaction is in fact a "four-wave mixing" process since there are four electro-magnetic waves involved, which includes the wave generated by the nonlinear polarization $\boldsymbol{P}^{(3)}$ in addition to the three incident waves. When the difference frequency of $\boldsymbol{E_1}$ and $\boldsymbol{E_2}$ is in resonance with the molecular vibration frequency $\delta\omega$ (that is, $\delta\omega=|\omega_1-\omega_2|$) the resonance effect will cause the molecule to oscillate coherently such that the polarization $\boldsymbol{P}^{(3)}$ will vary significantly with the vibration frequency $\delta\omega$. During this process, three frequency components ω_0, $\omega_0+\delta\omega$, and $\omega_0-\delta\omega$ will compose the scattered light. In this case, the scattered light with frequency $\omega_0+\delta\omega$ or $\omega_0-\delta\omega$ is enhanced by the coherence effect (Note that with $\boldsymbol{N}$ numbers of molecules emitting coherently, the increase in the emission intensity is not $\boldsymbol{N}$ times but rather $\boldsymbol{N}^2$ times in intensity). The scattered light with frequency $\omega_0+\delta\omega$ is called Coherent Anti-Stokes Raman Scattering (CARS) while the scattered light with frequency $\omega_0-\delta\omega$ is called Coherent Stokes Raman Scattering (CSRS). Given that it is not

easy to have a laser source with three different frequencies, the frequency of the field $\boldsymbol{E_0}$ usually coincides with either $\boldsymbol{E_1}$ or $\boldsymbol{E_2}$ (ω_1 or ω_2). Taking into account the phase of each light wave, Eq. (2) is rewritten as,

$$\text{CARS}: \boldsymbol{P}^{(3)}(\omega_1+\delta\omega)=\alpha\boldsymbol{E_1}(\omega_1)\boldsymbol{E}_1(\omega_1)\boldsymbol{E}_2^*(\omega_2) \quad (\omega_1+\delta\omega=\omega_1+\omega_1-\omega_2\ ,\ \omega_1>\omega_2) \tag{3a}$$

$$\text{CSRS}: \boldsymbol{P}^{(3)}(\omega_2-\delta\omega)=\alpha\boldsymbol{E}_1^*(\omega_1)\boldsymbol{E}_2(\omega_2)\,\boldsymbol{E}_2(\omega_2) \quad (\omega_1-\delta\omega=\omega_2+\omega_2-\omega_1\ ,\ \omega_1>\omega_2) \tag{3b}$$

Here, $\boldsymbol{E}^*$ is the phase conjugate of $\boldsymbol{E}$.

In Eq. (3a), the interaction of the photons of ω_1 and ω_2 with the molecule (lattice vibration) leads to the generation of a photon having frequency $\omega_1+\delta\omega$ through the 3rd order nonlinear optical process. In the CSRS process shown in Eq. (3b), the interaction of the photons of ω_1 and ω_2 with the lattice vibration leads to the generation of a photon with frequency ω_2 - $\delta\omega$ via the same optical process. In addition to the CARS and CSRS, four-wave mixing also leads to inverse Raman scattering (IRS), which is the annihilation of a ω_1 ($=\omega_1-\omega_2+\omega_2$) photon; or stimulated Raman gain scattering (SRGS), which is the creation of a ω_2 ($=\omega_2+\omega_1-\omega_1$) photon. The nonlinear polarization corresponding to each of these scattering processes are given by the following equations:

$$\text{IRS}: \boldsymbol{P}^{(3)}(-\omega_1)=\alpha\boldsymbol{E_1}^*(\omega_1)\boldsymbol{E}_2(\omega_2)\boldsymbol{E}_2^*(\omega_2) \quad (-\omega_1=-\omega_1+\omega_2-\omega_2\ ,\ \omega_1>\omega_2) \tag{3c}$$

$$\text{SRGS}: \boldsymbol{P}^{(3)}(\omega_2)=\alpha\boldsymbol{E_2}(\omega_2)\boldsymbol{E}_1(\omega_1)\boldsymbol{E}_1^*(\omega_1) \quad (\omega_2=\omega_2+\omega_1-\omega_1\ ,\ \omega_1>\omega_2). \tag{3d}$$

The IRS and SRGS processes represent two aspects of the energy exchange between the incident fields $\boldsymbol{E_1}$ and $\boldsymbol{E_2}$: In IRS we observe a reduction of intensity in $\boldsymbol{E_1}$ while in SRGS we observe an increase of $\boldsymbol{E_2}$ as a result of energy transfer from $\boldsymbol{E_1}$ to $\boldsymbol{E_2}$ through the coherent Raman process.

2.2 Principle of time-domain coherent Raman spectroscopy based on spectral focusing

For a coherent Raman spectroscopy system that uses two excitation light sources ω_1 and ω_2, two frequency-stabilized and frequency-tunable lasers are needed. This will make the system bulky. Moreover, the excitation lasers should have a narrow spectral linewidth (< 1 cm^{-1}), and a very efficient notch filter, having sufficient optical density and a sharp spectral edge, are required to filter out the Rayleigh scattering. To overcome this problem, a technique using the chirped frequency of the femtosecond laser was developed. Although the details of this technique will be explained below using CARS as an example, this technique is also applicable to other coherent Raman processes.

A femtosecond laser has a broad spectral bandwidth extending from several THz to a few tens of THz. The frequency of the femtosecond laser pulse can be chirped using a grating pair. After passing through the gratings, the chirped laser pulse is separated into two to produce Pump1 ($\boldsymbol{E_1}$) and Pump2 ($\boldsymbol{E_2}$) and combined again in an interferometer, where one pump pulse passes through an optical delay line. If the two pump pulses overlap with a time difference $\Delta\tau$, a $\Delta\tau$-dependent optical beat arising from the beat frequency will be generated. If this optical beat is incident onto a sample material, a frequency-chirped and up-converted CARS signal can be obtained, as seen on the left illustration in Fig.1. This technique for obtaining a narrow band signal from broadband, chirped pump pulses is

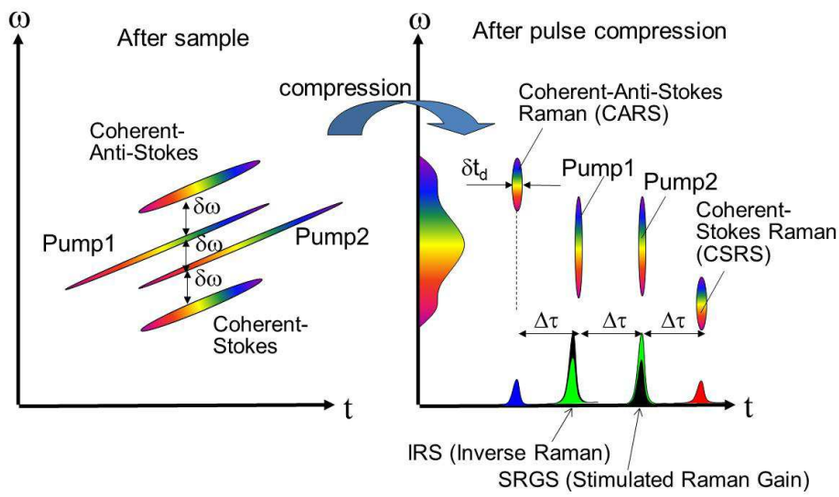

Fig. 1. Frequency chirped Pump1, Pump2, and coherent Raman emissions (Left), and those of after pulse compression (Right) in the time-frequency plane.

called "spectral focusing", reported by Hellerer *et al* in 2004 (Hellerer et al., 2004). Using a spectral focusing technique with a femtosecond laser, they successfully observed C−N Raman bands of nitroprusside [$Fe(CN)_5NO^{2-}$] at around 2160 cm^{-1} with three sharp peaks separated ~15 cm^{-1} apart from each other.

However, if the difference frequency, δω, in the CARS signal is small, the signal, Pump1 and Pump2 beams are spectrally overlapped and cannot be separated by dispersing these spectra as is usually done in Raman spectrum measurements. In addition, the CARS signal beam is almost collinear with the pump beams due to the phase-matching condition in the THz regime.

$$\mathbf{k}_{CARS}=2\mathbf{k}_1-\mathbf{k}_2\cong\mathbf{k}_1(\cong\mathbf{k}_2) \tag{4}$$

Here $\mathbf{k}_{CARS}$ is the wave vector of the CARS signal and $\mathbf{k}_1$ ($\mathbf{k}_2$) is that of Pump1 (Pump2). They can be separated only in time domain by pulse compression through the inverse chirping process, as shown by the right illustration in Fig. 1. The detection of the CARS signal in time-domain is possible using the up-conversion technique. Only one femtosecond laser is needed with this technique and neither a monochromater nor a filter is necessary. Likewise, it is possible to detect the CSRS signal of Pump2 at a frequency $\omega_2-\delta\omega$. Lastly, by means of the above technique, the IRS and SRGS signal can be detected by monitoring intensity changes in the coherent Raman scattering. The time-domain coherent Raman process resembles the chirped pulse amplification (CPA) technique, with which the frequency chirped pulse is amplified and compressed to obtain a high energy femtosecond laser pulses.

In time-domain coherent Raman spectroscopy, the frequency bandwidth of the detected coherent Raman signal is limited by the spectral bandwidth of the pump beams since the signal is the result of the difference frequency mixing of the two pump beams. On the other hand, the frequency resolution is determined by the reciprocal of the time-width ΔT of the two chirped optical pulses. The frequency resolution $\Delta\nu$ is given by

$$\Delta\nu(=\Delta\omega/2\pi)=1/\Delta T. \tag{5}$$

The time-width of the optical beat is maximum when the associated beat frequency (Raman frequency) is ν~0, and decreases proportionately with the increase of the beat frequency. Therefore, the frequency resolution Δν increases as the Raman frequency decreases. The highest frequency resolution obtainable at the low frequency limit for a femtosecond laser with a transform-limited pulse width of δ*t* and a chirp rate *b* is given by

$$\Delta\nu_{\mathrm{m}} = 1/\Delta T_{\mathrm{m}} = \delta\tau \cdot b, \tag{6}$$

where ΔT_{m} is the pulse duration of the chirped pump pulse. Accordingly, in order to get a good frequency resolution, one should use a laser with a narrow pulse width and be able to significantly stretch the pulse.

2.3 Experimental setup for time-domain coherent Raman spectroscopy

The schematic illustration of the experimental setup is shown in Fig. 2. Femtosecond pulses from a Ti: sapphire regenerative amplifier system (λ ~800 nm, δ*t* ~120 fs, 1 kHz, 800 μJ/pulse) were initially split into pump and probe pulses. The pump pulse was positively chirped with a grating-lens pair and stretched to about 30 ps. Using a Michelson-type interferometer, the stretched pump pulse was divided into two beams, Pump1 and Pump2, after which the two beams acquired a relative time-delay, Δτ, and were then recombined. The interference of the two pump beams produced an optical beat at the beams' instantaneous difference frequency. The interfering pump beams were then directed to the sample material. Subsequently, the pump beams were compressed to their original fs pulse widths using another grating pair. The frequency chirped CARS signal was also compressed and separated from Pump1 by Δτ in time domain. The CARS signal was then up-converted to ~400-nm wavelength through sum frequency generation (SFG) with the probe pulse using a BBO crystal. The up-converted signal was then detected by a GaP photodiode. In order to have a high SNR, either Pump1 or Pump2 should be modulated by a mechanical chopper and the photodiode signal can then be detected by a lock-in amplifier.

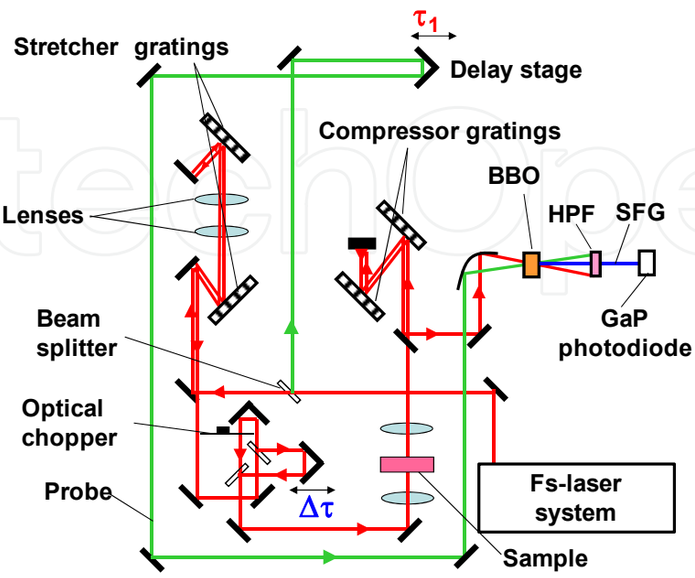

Fig. 2. Experimental setup for time-domain coherent Raman spectroscopy

Figure 3(a) shows the SHG cross-correlation signal for stretched Pump1 and Pump2 with a time difference, whose beat frequency is 736 GHz. Figure 3(b) shows the Fourier transformed SHG cross-correlation signal for stretched Pump1 and Pump2 with various $\Delta\tau$ values. By plotting the observed beat frequencies against the optical delay $\Delta\tau$ we can determine the chirp rate b of the pump pulses. From Fig. 3(b) it is also found that the spectral line width of the optical beat increases with increasing beat frequency, resulting in poor spectral resolution of the time-domain coherent Raman spectra at higher frequencies. The frequency resolution, $\Delta\nu_m$, in the low frequency limit ($\nu \sim 0$) is calculated to be 0.02 THz for the present system with the pulse width δt = 120 fs and the chirp rate b =0.18 THz/ps. The useful bandwidth of the CARS measurement system estimated by the optical beat measurement is about 5 THz. The low-frequency limit of the CARS measurement is determined by the pulse width of the pump laser after the compression and is about 0.2 THz in the present system.

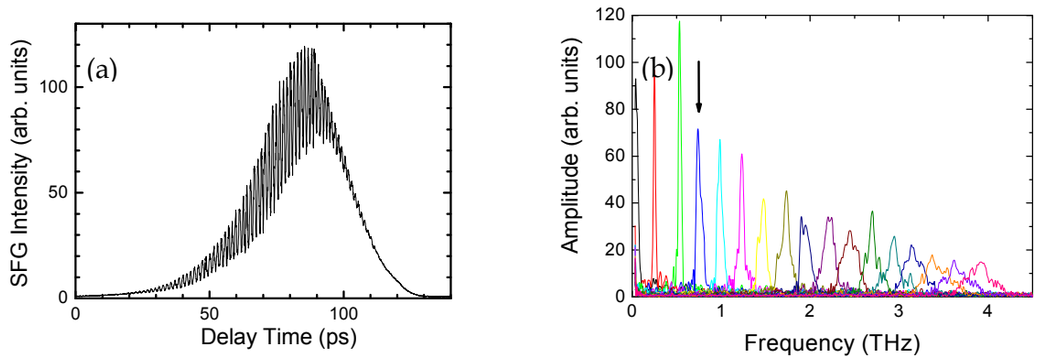

Fig. 3. (a) SHG cross-correlation signal of stretched Pump1 and Pump2. (b) Fourier transformed cross-correlation signal of stretched Pump1 and Pump2 with various $\Delta\tau$. The Fourier transformed spectrum of SHG correlation signal shown in (a) is indicated by a vertical arrow.

3. Time-domain coherent Raman spectroscopy

3.1 Time-domain coherent anti-Stokes Raman spectroscopy (CARS) for GaSe

Figure 4 shows the CARS spectrum measured from a β-GaSe single crystal (*c*-cut, 1 mm thickness) sample (Tani et al., 2010). The spectrum shown in Fig. 4 was obtained by "peak-scanning", where the time-delay τ_1 for the probe and the relative time difference, $\Delta\tau$, between Pump1 and Pump2 are simultaneously scanned while the ratio of the two delays, $\tau_1/\Delta\tau$, was kept equal to 2 (τ_1=2 $\Delta\tau$). In effect, the frequency shift of the CARS signal with respect to the change of the difference frequency $\delta\omega$ was investigated. To increase the SNR the "peak-scanned" spectrum was averaged for 10 times.

On the broad, non-resonant background spectrum a resonance can be seen near 0.6 THz (~20 cm^{-1}), coming from the lowest Raman-active optical mode (E_{2g} mode) in β-GaSe (Wieting & Verble, 1972). The non-resonant coherent Raman signal originates from electronic response of the sample and is not strongly frequency dependent. The resonant CARS spectrum is not symmetric but has a dispersion-type structure. This is explained by the interference between the components from the non-resonant (real and constant with frequency) and the resonant nonlinear optical susceptibility (Levenson, 1974). The CARS signal intensity is proportional to

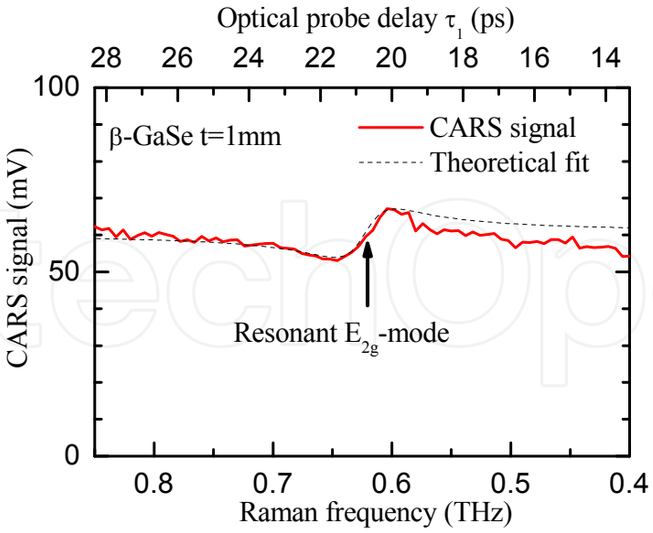

Fig. 4. CARS spectrum of GaSe showing the optical phonon band near 0.6THz

$$|\chi^{(3)}|^2 = |\chi_N^{(3)} + \chi_R^{(3)}|^2$$

$$= |\chi_N^{(3)}|^2 + \chi_N^{(3)} \frac{a(\omega_d - \omega_R)}{(\omega_d - \omega_R)^2 + \Gamma^2} + \frac{a^2}{(\omega_d - \omega_R)^2 + \Gamma^2} \tag{7}$$

Here, $\chi_N^{(3)}$ is the non-resonant third order susceptibility, which is assumed to be a real constant, while the resonant third order susceptibility $\chi_R^{(3)}$ is given in the following form:

$$\chi_R^{(3)}(\omega_d = \omega_p - \omega_S) = \frac{a(\omega_d - \omega_R + i\Gamma)}{(\omega_d - \omega_R)^2 + \Gamma^2} \tag{8}$$

Here, $\omega_d = \omega_p - \omega_S > 0$ is the difference frequency between the pump (Pump1) and Stokes (Pump2), ω_R is the Raman resonance frequency, Γ is the Raman linewidth, and a is the constant associated with the magnitude of the resonance. When the non-resonant contribution is large compared to the resonant one, we can neglect the last term in Eq.(7). Then we obtain

$$\text{CARS} \propto |\chi_N^{(3)}|^2 + 2\chi_N^{(3)} \frac{a(\omega_d - \omega_R)}{(\omega_d - \omega_R)^2 + \Gamma^2} = |\chi_N^{(3)}|^2 + 2\chi_N^{(3)} \frac{a\Delta\omega}{\Delta\omega^2 + \Gamma^2} \tag{9}$$

Here, $\Delta\omega = \omega_d - \omega_R$ is the detuning from the resonant Raman frequency. The schematic illustration of the CARS signal interfering with the resonant and non-resonant components is shown in Fig. 5 The curve fit using eq.(3) is shown in Fig. 4 as the dashed line. We have estimated the Raman linewidth Γ = 0.02 THz (=0.67 cm^{-1}) and the ratio of the resonant to the non-resonant contribution, given by the parameter $a/(\Gamma\chi_N^{(3)})$, to be 12%. The discrepancy between the theoretical curve fit and the observed spectrum in the low-frequency side is due to the drift of the non-resonant background signal caused by the fluctuation of the laser intensity.

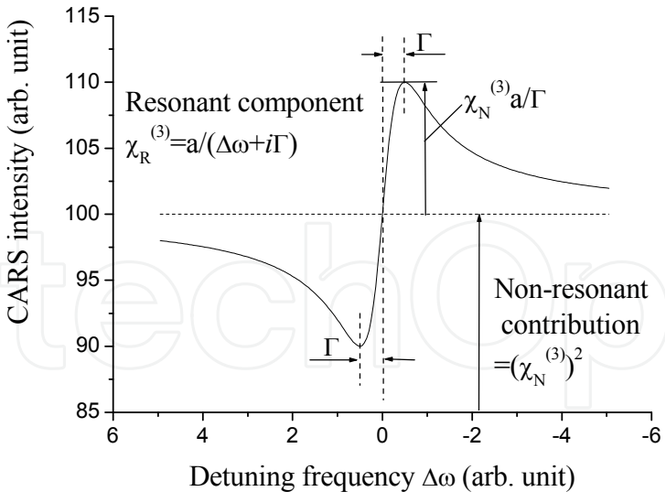

Fig. 5. The structure of CARS spectrum resulting from interference between the non-resonant and resonant components

3.2 Time-domain inverse Raman spectroscopy (IRS) for GaSe

Figure 6 shows the inverse Raman spectrum of the β–GaSe sample. The total pump power incident on the sample was about 1 mW. The signal loss of Pump1 was detected using lock-in techniques by modulating Pump2 with a mechanical chopper. The IRS spectrum was taken by scanning the Pump2, $\Delta\tau$, with the probe optical delay set at the maximum SFG signal . As can be seen from Fig. 6, there are resonance peaks around 0.6 and 4.2 THz due to the E_{2g} and A_{1g} optical phonon modes, respectively. The resonance peak expected at 1.8 THz corresponding to an optical phonon (E_{1g}-mode) in GaSe was not observed, probably due to the weak Raman scattering cross section. The inverse Raman signal is one order stronger than the CARS signal. Accordingly, the SNR of the inverse Raman signal is also larger. The reason for this is not clear at present.

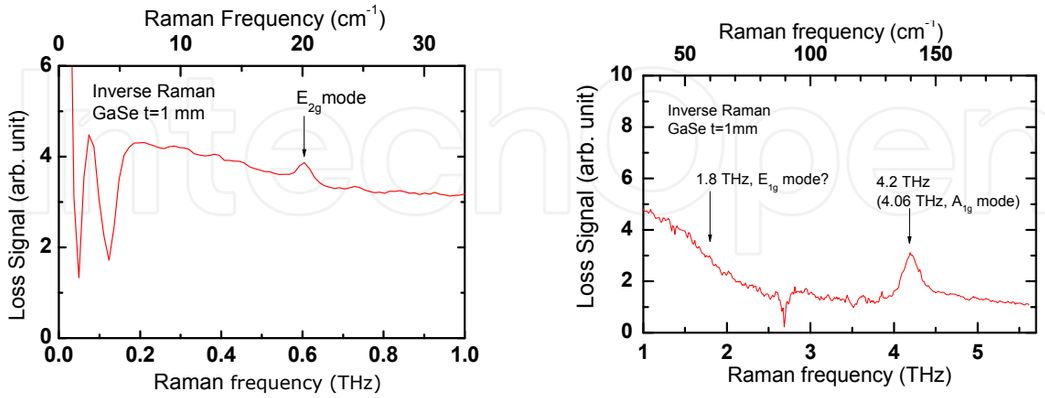

Fig. 6. Inverse Raman spectra of GaSe

One of the advantages of the time-domain IRS (and SRGS) in comparison with the time-domain CARS (or CSRS) is that it is not necessary to scan the optical delay τ_1 of the probe light simultaneously with $\Delta\tau$. In addition, the IRS spectrum is symmetric about the

resonance frequency while that of CARS is not symmetric (dispersive shape). This is because the signal in an IRS spectrum corresponds to the imaginary part of the 3rd order nonlinear susceptibility (the same as the spontaneous Raman signal) while that of CARS corresponds to the real part, and this is the reason why it interferes with the signal from the real non-resonant nonlinear susceptibility. The non-resonant background signal is also dominant as in CARS and is probably due to other non-resonant four-wave mixing processes. Therefore, it is necessary to suppress this non-resonant background signal when performing spectroscopy of biomolecules and imaging where a higher SNR is required.

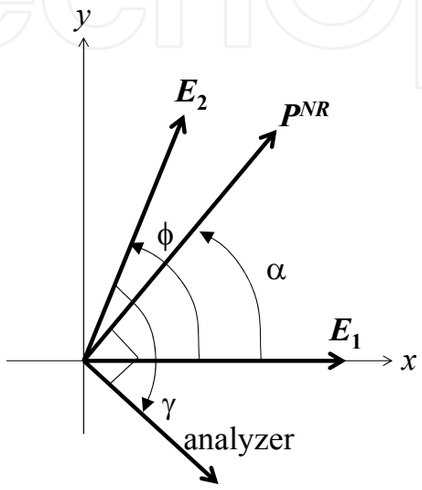

Fig. 7. Polarization vectors of Pump1 ($\boldsymbol{E}_1$) and Pump2 ($\boldsymbol{E}_2$), the non-resonant IRS signal ($\boldsymbol{P}^{NR}$) and the analyser polarizer.

The polarized CARS (P-CARS) technique (Oudar et al., 1979; Cheng et al., 2001) can be applied to the inverse Raman measurement in order to suppress the non-resonant background signal. This is achieved by controlling the relative polarization angle between Pump1 and Pump2; that is, adjusting the polarization direction of the non-resonant and resonant signals. Owing to the polarization difference, it is possible to remove the polarization component of the non-resonant signal by placing a polarizing filter in front of the detector. The principle of polarization IRS method (P-IRS) is outlined as follows. Consider that Pump1 is linearly polarized along the x-axis and Pump2 is polarized along a direction, an angle ϕ relative to the x-axis as shown Fig.7. When the beat frequency generated by the two pump beams is resonant with a molecular vibration or an optical phonon vibration, the interaction of the pump beam in the sample induces a third order nonlinear polarization that contains a non-resonant part, $\boldsymbol{P}^{NR}$, and a resonant part, $\boldsymbol{P}^{R}$. The x and y components of the non-resonant part contributing to IRS can be written as

$$P_x^{NR} = 3\chi_{1111}^{NR} E_1^{\ *} E_2\ E_2^{\ *} \cos^2\phi\,,$$

$$P_y^{NR} = 3\chi_{2112}^{NR} E_1^{\ *} E_2\ E_2^{\ *} \cos\phi \sin\phi \tag{10}$$

Similarly, the x and y components of the resonant part can be written as

$$P_x^R = 3\chi_{1111}^R E_1^* E_2 \, E_2^* \cos^2\phi \,,$$

$$P_y^R = 3\chi_{2112}^R E_1^* E_2 \, E_2^* \cos\phi \sin\phi \tag{11}$$

In the absence of electronic resonance, χ^{NR} is a real quantity and independent of frequency. In this case the depolarization ratio of the non-resonant IRS field is

$$\rho^{NR} = \frac{\chi_{2112}^{NR}}{\chi_{1111}^{NR}} = \frac{1}{3} \tag{12}$$

$\boldsymbol{P}^{NR}$ is therefore linearly polarized with an angle α relative to the x axis,

$$P^{NR} = 3\chi_{1111}^{NR} E_1^* E_2 \, E_2^* \cos^2\phi / \cos\alpha \tag{13}$$

where the angle α is related to ϕ by $\tan\alpha = \rho^{NR} \tan\phi$.
The non-resonant background can be removed by placing an analyzer in front of the detector, with its polarization perpendicular to $\boldsymbol{P}^{NR}$. The total projection of the two components of $\boldsymbol{P}^{R}$ [Eq. (11)] along the direction perpendicular to $\boldsymbol{P}^{NR}$ can be written as

$$P_\perp = 3\chi_{1111}^R E_1^* E_2 \, E_2^* (\cos^2\phi \sin\alpha - \rho^R \cos\phi \sin\phi \cos\alpha) \tag{14}$$

Here,

$$\rho^R = \frac{\chi_{2112}^R}{\chi_{1111}^R} \tag{15}$$

is the depolarization ratio of the resonant IRS field, and is equal to the spontaneous Raman depolarization ratio in the absence of electronic resonance.

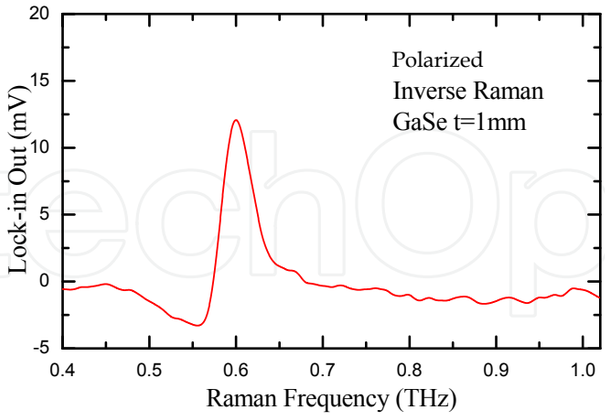

Fig. 8. Polarized inverse Raman signal of GaSe from 0.4 to 1.0 THz

Even as this technique causes a slight reduction of the resonant signal, a large amount of the non-resonant signal is suppressed. Figure 8 shows the inverse Raman spectrum using the polarization technique. As can be seen from the figure, the non-resonant component is well suppressed and the resonance peak is clearly seen at the optical phonon mode frequency around 0.6 THz.

4. Extension of measurement bandwidth

The measurement bandwidth is dependent on the spectral bandwidth and thus the associated pulse width of the femtosecond laser. Thus, using a narrow pulse width femtosecond laser will give a broad measurement bandwidth. However, when using very short pulses (less than 100 fs), special care must be taken to suppress higher order dispersion in the stretcher configuration. With a grating pair such as the one shown in Fig.2 (the compressor part), optical pulses with negative chirp can be obtained. When a lens pair is inserted between the grating pair, the spatial image of the optical beam is inverted and a negative chirp is then reverted to a positive chirp. However, the insertion of a lens pair introduces higher order dispersion and spherical aberration, which cannot be compensated by the grating pair compressor. As a result, the pulse width after compression is broadened with the higher order dispersion and the time-resolution in the detection system deteriorates. To avoid dispersive optics in the stretcher system we adopted Öffner configuration (Öffner, 1971; Cheriaux et al., 1996), which consists of a grating and a combination of concave, convex and roof mirrors as shown in Fig. 9. The optical pulses hit the grating and the aspheric mirrors four times. By changing the offset distance Z_1 of the grating position we can control the positive dispersion of the optical pulses.

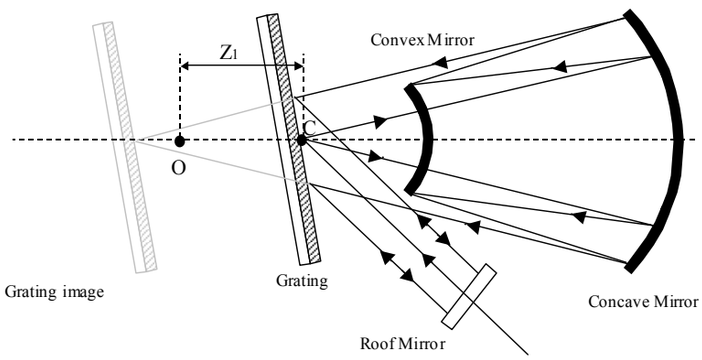

Fig. 9. The Öffner configuration used as the stretcher. The point *O* is the center of curvature of both mirrors. The point *C* is the incident position of the optical pulses on the grating. The point C lies on the incidence plane of the optical pulses on the grating.

Figure 10 shows the measured inverse Raman spectrum from the β–GaSe using femtosecond laser pulses with a pulse width of 40 fs in the transform-limited condition. The vertical axis of the graph is the optical power loss in Pump1, corresponding to the inverse Raman signal, while the horizontal axis is the relative time-delay between the two pump pulses, which determines the beat frequency. The sharp peak at the zero time-delay is the burst signal of the overlapping pump pulses, which corresponds to zero-beat frequency. The small and sharp peak at 1.1 ps (~0.6 THz) is the optical phonon mode (E_{2g} mode), corresponding sliding motion of layers with its plane perpendicular to the *c*-axis of GaSe. The apparent peak at 7.9 ps (4 THz) is the fully symmetric phonon mode (A_{1g} mode) and the peak at 18.7 ps (9.3 THz) is another Raman active mode (A_{1g} mode) (Wieting & Verble, 1972). Based on these bands and the associated non-resonant background signal, the frequency bandwidth of this system is estimated to be 15 THz (corresponding to ~30 ps time delay).

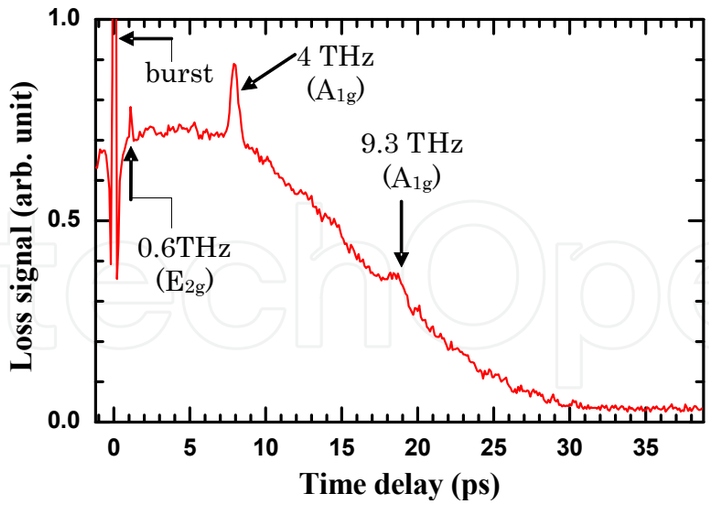

Fig. 10. Inverse Raman signal from GaSe (*c*-cut, t = 1 mm) measured using a 40 fs pulse width laser

5. Problem and future plan

A crucial aspect of the coherent Raman spectroscopy system is its utilization of a femtosecond laser in conjunction with a novel time-domain detection scheme to acquire the sub-THz to THz coherent Raman spectrum. However, low signal strength from samples like biomolecules necessitates improving the SNR of the system. The efficiency of coherent Raman scattering and the SFG process in the signal detection is proportional to the cube and square of the excitation intensity, respectively. Therefore, the coherent Raman scattering signal detected in time-domain is proportional to the 4^{th} power of the excitation intensity. Laser intensity fluctuations in turn, cause large fluctuations in the signal. This deteriorates the SNR, even if the signal itself is large. Moreover, the large fluctuation of the non-resonant signal compared to the resonant signal due to vibrational modes also results in a low SNR. In order to address these issues, the following points may be considered: (1) use a high repetition rate laser, (2) use balanced detection or obtain the difference between the signal and the reference, and (3) establish ways of measuring the differential signal in the time delay of Pump1 and Pump2 (equivalent to the differential signal in the frequency domain) through the modulation of their optical path lengths. If the repetition rate of the pump laser is too high, as in the case of a mode-locked Ti:sapphire laser oscillator (having typical repetition frequencies of 50~100 MHz), the energy per pulse is too small and the coherent Raman signal strength is too weak resulting to a low SNR. For this reason, the optimum pump source might be a femtosecond laser amplifier system with a repetition rate of ~100-kHz and with an energy per pulse of a few μJ, in order to maintain sufficient excitation intensity.

6. Conclusion

THz time-domain coherent Raman spectroscopy system using "spectral focusing" of a broadband femtosecond laser source was introduced. Although the system is still in its

development stage, sufficient SNR was obtained using a GaSe sample. Additionally, it promises to be a reliable measurement technique for background light and fluorescence studies since the signal is gated in the time domain. Lastly, improving the SNR characteristics of the system will make it feasible for applications in the spectroscopy and imaging of biomolecular samples.

7. Acknowledgment

The Authors are grateful to the "SAKIGAKE (PREST)" Grant in the research area "Life Phenomena and Measurement Analysis" by the Japan Science and Technology Agency, and the Grants-in-Aid for Scientific Research (KAKENHI) (B) program by the Japan Society for the Promotion of Science (JSPS).

8. References

Brooks, B. & Karplus, M. (1985). Normal Modes for Specific Motions of Macromolecules: Application to the Hinge-Bending Mode of Lysozyme. *Proceedings National Academy of Sciences*, Vol.82, No.15, (August 1985), pp. 4995-4999

Cheng, J.–X.; Book, L. & Xie, X. S. (2001). Polarization Coherent Anti-Stokes Raman Scattering Microscopy. *Optics Letters*, Vol.26, No.17, (September 2001), pp. 1341-1343

Cheriaux, G.; Rousseau, P.; Salin, F.; Chambaret, J. P.; Walker, B. & L. F. Dimauro. (1996) Aberration-free Stretcher Design for Ultrashort-pulse Amplification. *Optics Letters,* Vol.21, No. 16, (March 1996), pp. 414-416

Chou, K.-C. (1985) Low-frequency Motions in Protein Molecules. *Journal of Biophysics*, Vol.48, No.2, (August 1985), pp. 289-297

Chou, K.-C. (1988) Low-frequency Collective Motion in Biomacromolecules and its Biological Functions. *Biophysical Chemistry*, Vol.30, No.1, (May 1988), pp. 3-48

Genzel, L.; Keilmann, F.; Martin, T. P.; Winterling, G.; Yacoby, Y.; Frohlich, H. & Makinen, M. (1976). Low-Frequency Raman Spectra of Lysozyme. *Biopolymers*, Vol.15, No.1, (January 1976), pp. 219-225

Go, N.; Noguti, T. & Nishikawa, T. (1983). Dynamics of A Small Globular Protein in Terms of Low-frequency Vibrational Modes. *Proceedings National Academy of Sciences*, Vol.80, No. 12, (June 1983), pp. 3696-3700

Hangyo, M.; Tani, M. & Nagashima, T. (2005). Terahertz Time-Domain Spectroscopy of Solids: A Review. *International Journal of Infrared and Millimeter Waves*, Vol.26, No.12, (December 2005), pp. 1661-1690

Hellerer, T.; Enejder, A. M. K. & Zumbusch, A. (2004). Spectral Focusing: High Spectral Resolution Spectroscopy with Broad-bandwidth Laser Pulses. *Applied Physics Letters,* Vol.85, No.25, (March 2004), pp. 25-27

Kawase, K. (2004). Terahertz Imaging For Drug Detection and Large-scale Integrated Circuit Inspection. *Optics & Photonics News,* Vol.15, No.10, (October 2004), pp. 34-39

Kawase, M.; Saito, T.; Ogawa, M.; Uejima, H.; Hatsuda, Y.; Kawanishi, S.; Hirotani, Y.; Myotoku, M.; Ikeda, K.; Takano, K.; Hangyo, M.; Yamamoto, K. & Tani, M. (2009).

Terahertz Absorption Spectra of Original and Generic Ceftazidime. *Analytical Sciences,* Vol.25, No.12, (November 2009), pp. 1483-1485

Korter, T. M.; Balu, R.; Campbell, M. B.; Beard, M. C.; Gregurick, S. K. & Heilweil E. J. (2006). Terahertz Spectroscopy of Solid Serine and Cysteine. *Chemical Physics Letters,* Vol.418, No.1, (November 2005), pp. 65-70

Levenson, M. C. (1974). Feasibility of Measuring the Nonlinear Index of Refraction by Third-order Frequency Mixing. *IEEE Journal of Quantum Electronics,* Vol.10, No.2, (February 1974), pp. 110-115

Öffner, A. U.S. patent 3,748,015 (1971)

Okajima, H. & Hamaguchi, H. (2009). Fast Low Frequency (Down to 10 cm^{-1}) Multichannel Raman Spectroscopy Using an Iodine Vapor Filter. *Applied Spectroscopy,* Vol.63, No.8 (August 2009), pp. 958-960

Oudar, J. L.; Smith, R. W. & Shen, Y. R. (1979). Polarization-sensitive Coherent Anti-Stokes Raman Spectroscopy. *Applied Physics Letters*, Vol.34, No.11, (June 1979), pp. 758-760

Taday, P. F.; Bradley, I. V.; Arnone, D. D. & Pepper, M. (2003). Using Terahertz Pulse Spectroscopy to Study the Crystalline Structure of a Drug: A Case Study of the Polymorphs of Ranitidine Hydrochloride. *Journal of Pharmaceutical Science,* Vol.92, No.4, (April 2003), pp. 831-838

Tani, M.; Yamaguchi, M.; Miyamaru, F.; Yamamoto, K. & Hangyo, M. (2004). Spectroscopy of Biomolecules using Terahertz Electromagnetic Pulse– Measurement of the Low Vibration Mode of Amino Acids using Terahertz Time-domain Spectroscopy. *Optical Alliance*, Vol.15, No.1, (2004), pp.9-14 (in Japanese)

Tani, M.; Koizumi, T.; Sumikura, H.; Yamaguchi, M.; Yamamoto, K. & Hangyo, M. (2010). Time-Domain Coherent Anti-Stokes Raman Scattering Signal Detection for Terahertz Vibrational Spectroscopy Using Chirped Femtosecond Pulses. *Applied Physics Express*, Vol.3, (July 2010), pp. 072401-1-072401-3

Tani, M. & Hangyo, M. (2010). Terahertz Wave Emission and Application using a Femtosecond Solid-state Laser in the Special Issue on Wavelength Conversion Technology with Solid-state Lasers and its Applications. *Optical Alliance*, Vol.21 No.6, (2010), pp.15-20 (in Japanese)

Urabe, H.; Sugawara, Y.; Ataka, M. & Rupprecht, A. (1998). Low-Frequency Raman Spectra of Lysozyme Crystals and Oriented DNA Films: Dynamics of Crystal Water. *Biophysical Journal*, Vol.74, No.3, (March 1998), pp. 1533–1540

Walther, M.; Fischer, B. M. & Jepsen, P. U. (2003). Noncovalent Intermolecular Forces in Polycrystalline and Amorphous Saccharides in the Far Infrared. *Chemical Physics*, Vol.288, No.2, (March 2003), pp. 261-268

Wieting, T. J. & Verble, J. L. (1972). Interlayer Bonding and the Lattice Vibrations of β-GaSe. *Physics Review B,* Vol.5, No.4, (February 1972), pp. 1473-1479

Yamaguchi, M.; Miyamaru, F.; Yamamoto, K.; Tani, M. & Hangyo, M. (2005). Terahertz Absorption Spectra of L-, D-, and DL-alanine and their Application to Determination of Enantiometric Composition. *Applied Physics Letters,* Vol.86, No.5, (January 2005), pp. 053903-1-053903-3.

Yamamoto, K.; Tominaga, K.; Sasakawa, H.; Tamura, A.; Murakami, H.; Ohtake, H. & Sarukura, N. (2005). Terahertz Time-Domain Spectroscopy of Amino Acids and Polypeptides. *Biophysical Journal,* Vol.89, No.3, (September 2005), pp. L22-L24

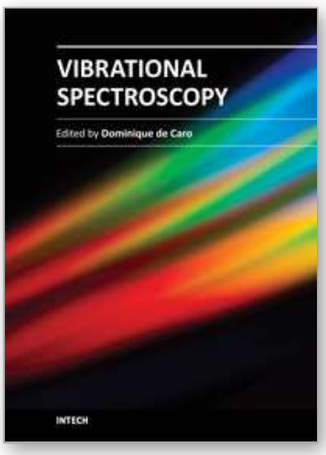

Vibrational Spectroscopy

Edited by Prof. Dominique De Caro

ISBN 978-953-51-0107-9
Hard cover, 168 pages
Publisher InTech
Published online 24, February, 2012
Published in print edition February, 2012

The infrared and Raman spectroscopy have applications in numerous fields, namely chemistry, physics, astronomy, biology, medicine, geology, mineralogy etc. This book provides some examples of the use of vibrational spectroscopy in supramolecular chemistry, inorganic chemistry, solid state physics, but also in the fields of molecule-based materials or organic-inorganic interfaces.

InTech Europe
University Campus STeP Ri
Slavka Krautzeka 83/A
51000 Rijeka, Croatia
Phone: +385 (51) 770 447
Fax: +385 (51) 686 166
www.intechopen.com

InTech China
Unit 405, Office Block, Hotel Equatorial Shanghai
No.65, Yan An Road (West), Shanghai, 200040, China
中国上海市延安西路65号上海国际贵都大饭店办公楼405单元
Phone: +86-21-62489820
Fax: +86-21-62489821

IntechOpen